Surface Science 677 (2018) 18–25

Contents lists available at ScienceDirect

Surface Science

journal homepage: www.elsevier.com/locate/susc

Surface phase diagrams of titanium in Oxygen, Nitrogen and Hydrogen environments: A first principles analysis

Sanjubala Sahoo[a,*], S. Pamir Alpay[a,b], Rainer J. Hebert[a,c]

[a] Department of Materials Science and Engineering and Institute of Materials Science, University of Connecticut, Storrs, CT 06269, USA
[b] Department of Physics, University of Connecticut, Storrs, CT 06269, USA
[c] Pratt & Whitney Additive Manufacturing Center, University of Connecticut, Storrs, CT 06269, USA

ARTICLE INFO

Keywords:
Ti surface
Oxide
Nitride and hydride phase
Surface phase diagram
Ab-initio thermodynamics
Density functional theory

ABSTRACT

Density functional theory and *ab initio* thermodynamics studies are performed to investigate the interaction of oxygen, nitrogen and hydrogen molecules with hexagonal close packed Ti (0001) surfaces. The system is modeled as a slab where the concentration of the adsorbed atoms is systematically increased and the most favorable configuration is determined based on total energy comparisons. Varying tendencies are observed for the ground state structures of oxygen, nitrogen and hydrogen adsorption. Oxygen and hydrogen atoms are found to be adsorbed on the surface with increasing concentration and tend to migrate to interior layer only after surface saturation. However, nitrogen prefers to migrate into the interior layers. For all elements, the favorable position in the interior layers is the octahedral interstitial site. Taking into account the partial pressure of oxygen, nitrogen and hydrogen and the effect of temperature, we develop surface phase diagrams that display stable surface configurations. Our studies provide an atomic insight into the structure of the surface scale, passivation effects, and surface tension of Ti for advanced powder manufacturing processes and applications in catalysis.

1. Introduction

Metal surfaces play an important role in solid state chemistry, condensed matter physics, and materials science and engineering [1–3]. Catalysis and corrosion are technologically relevant and are well-known examples of phenomena that depend on metal surface characteristics. But many other examples exist where metal surfaces control mechanisms and properties: wear of metallic parts, paint adhesion, and more recently also the flow of powders during additive manufacturing. The surfaces of metallic powder particles represent contact areas between particles in powder beds. The dynamics of powder beds during raking or rolling are simulated using discrete element models. These models depend on the atomic level interactions between contacting powder particles and these interactions depend on the reactions occurring at the particle surfaces. At a microscopic level metal surfaces offer diffusion and reaction pathways either on the surfaces or between the surfaces and the atmospheric environments. The reaction pathways and kinetics associated with surfaces generally differ from those in the bulk and indeed are responsible for the surface-controlled phenomena.

Among the interactions between metal surfaces and atmospheric environments the reactions between oxygen and nitrogen molecules and the surfaces is very important, simply because those gases are the major constituents of the atmosphere. Hydrogen gas is furthermore relevant due to the very small size of hydrogen atoms that often poses challenges to material behavior when hydrogen atoms diffuse interstitially. Upon contact with a metal surface, these atmospheric molecules undergo chemical and physical changes including dissociation and charge exchange phenomena. Such processes result in a change in the surface potential and interfere with the general properties of the surfaces. Therefore, developing an understanding of the chemistry of base metal surfaces is important for controlling the chemical reactions, catalytic properties, and also for the design and engineering of surfaces for corrosion protection. The importance of metal surfaces exposed to O_2, N_2 or H_2 lies in the oxidation and corrosion processes where the surface changes from a metallic state to either an oxide, nitride or hydride. The surface stoichiometry is a function of temperature and partial pressure of the gas.

Of all metal surfaces, titanium (Ti) surfaces are highly relevant for studies of interactions with gases. On one hand, Ti-based alloys are used abundantly in aerospace, chemical, as well as biomedical industries due to their good corrosion resistance, light weight and high strength, and are thus technologically highly relevant [4–7]. On the other hand, Ti is

* Corresponding author.
E-mail address: sanjubala.sahoo@uconn.edu (S. Sahoo).

https://doi.org/10.1016/j.susc.2018.05.007
Received 16 February 2018; Received in revised form 31 March 2018; Accepted 14 May 2018
Available online 26 May 2018
0039-6028/

a highly reactive metal and is prone to oxidation and corrosion in oxygen, nitrogen and hydrogen surroundings, which ultimately affects its thermal stability and mechanical strength [6,8,9]. In fact, Ti has a high affinity for adsorption of oxygen, nitrogen or hydrogen molecules, which results in the dissociation of the gaseous molecules to their atomic components and the formation of surface oxide, nitride and hydride compounds [10–13].. Experimentally, several studies exist on the oxidation of Ti that demonstrate the possibility of a variety of stoichiometries and oxidation states [14–20]. These depend on the ambient temperature and partial pressure of oxygen in the environment. TiO_2, TiN, TiH_2 are the native (equilibrium) oxide, nitride and hydride compounds for Ti, respectively. Although numerous experimental and theoretical studies exist for TiO_2, TiN and TiH_2 compounds and the conditions for their formation [21–26], there needs to be a better understanding of the bonding and atomic structure of Ti-O, Ti-N, and Ti-N interfaces and Ti surfaces at high temperatures at varying partial pressures of O, N, and H.

With this study we aim to provide an atomistic understanding of the interaction of O_2, N_2 and H_2 with Ti surfaces. Specifically, we investigate the formation of different oxide, nitride and hydride phases and their stability with varying oxygen, nitrogen and hydrogen concentrations and temperature. We develop an electronic structure based methodology for the interaction of O, N and H with HCP Ti surface where the ground state properties of Ti-(O, N, H) systems for various compositions and their thermodynamic stability are investigated.

The results of this study are relevant for applications involving Ti and surface reactions with air or vacuum. The results apply to a wide range of technologies, for example, metal additive manufacturing [27–29] of Ti or heterogeneous catalysis where the oxide, nitride or hydride surfaces of Ti have indicated high catalytic activity for various chemical reactions [26,30–33].

2. Computational method and theoretical approach

The theoretical methodology employed in this study consists of a combination of density functional theory (DFT) and *ab initio* thermodynamics [34]. The DFT total energies are taken as input for the thermodynamics analysis. We are specifically interested in the interactions between HCP (α-phase) Ti surfaces with oxygen, nitrogen and hydrogen. The (0001) surface of HCP Ti is the primary surface for our study as this is the highly stable compared to other crystallographic planes of Ti [35].

2.1. DFT calculations

The DFT calculations are performed with generalized gradient approximation (GGA) for the exchange and correlation functional parameterized by Perdew-Burke-Erzernhof [36]. Further, GGA has been proved to be a very reasonable approximation for transition metal systems [37,38]. The calculations are performed using the VASP (Vienna *ab initio* Simulation Package) [39,40]. The projector augmented wave (PAW) method [41] is used for the core electron interactions. We especially focus on HCP (0001) Ti because the basal plane (0001) is the most stable and hence is more probable in nature [35]. The surface is modeled using a slab cut perpendicular to the *z*-direction from the HCP bulk of lattice parameters: $a = 2.92$ Å and $c = 4.63$ Å, which are the lowest energy lattice parameters obtained in GGA and in good agreement with experimental data [42]. The slab is modeled with 10 atomic layers with each layer containing 9 Ti atoms (with 3 × 3 size of 2-dimensional hexagonal units) along the *z*-direction as shown in Fig. 1. The semi-infinite nature of the slab is maintained by applying the periodicity along the surface plane (here, along the *x*- and *y*- directions) while along the *z*-direction, i.e., the direction perpendicular to the surface, a vacuum thickness of 16 Å is fixed. This is sufficient to minimize the interaction between the images. Furthermore, a dipole correction is applied along the *z*-direction in order to ensure proper

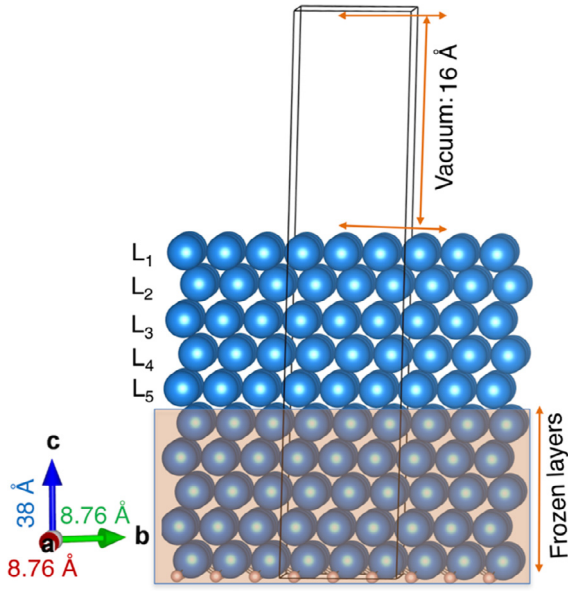

Fig. 1. Optimized geometry of Ti(0001) surface with the periodic images along the longitudinal directions and with 10 atomic layers along the transverse direction where the bottom Ti (blue) layer is passivated by H atoms (magenta balls). The shaded region illustrates the frozen layers. The layers L_1-L_5 indicate the Ti layers which are allowed for full optimization.

convergence of electrostatic potential on surfaces. The current slab model has two equivalent (0001) surfaces. Since the molecular adsorption is performed on one of the surfaces, the other (0001) surface is kept chemically inactive by passivating hydrogen atoms. Five consecutive layers of Ti facing the passivating surface is kept fixed (shown as shaded region in Fig. 1) to the bulk equivalent positions and atoms in other five layers (labelled as L_1 to L_5 in Fig. 1) are allowed to relax for geometrical optimization. The integration over the Brillouin zone is hence carried out with a 4 × 4 × 1 *k*-points mesh in the reciprocal space. All calculations are performed with a plane wave energy cutoff 400 eV with a tolerance for total electronic energy convergence criteria set to 10^{-7} eV and the tolerance in energy for ionic displacements set to 10^{-6} eV.

2.2. Thermodynamics from total energy considerations

In order to consider the effect of temperature (T) and pressure (p), the *ab initio* thermodynamics [34] formalism is implemented where the total energies obtained from DFT are taken as input for the thermodynamics analysis. The analysis is based on the physical quantity, namely, the surface free energy (γ). From thermodynamic consideration, γ is a function of temperature (T) and the surrounding partial pressure of the specific element (p). The surface energy can be written as;

$$\gamma(T, p) = \frac{1}{2A}[G - \mu_{Ti}(T, p)], \quad (1)$$

where G is the Gibbs free energy and μ_{Ti} is the chemical potential of Ti. In the presence of a X_2 gaseous environment (X = O, N or H), the adsorbed gas on Ti surface should be in thermodynamic equilibrium with both the Ti surface and the gaseous environment. Hence, Eq. (1) for a slab model leads to:

$$\gamma(T, p) = \frac{1}{2A}[G(\text{slab}) - n_{Ti}\,\mu_{Ti}(T, p) - n_X\,\mu_X(T, p)], \quad (2)$$

where it is assumed that one species of X_2 is adsorbed at a time. n_{Ti} and n_X are the number of Ti atoms and X atoms, respectively. The surface area of the slab is given by A. Neglecting configurational entropy effects

(which play a major role for multi-component alloy systems), the free energy term G(slab) can be replaced by total energy E^{Total}(slab), which can be obtained from atomistic or electronic models such as DFT. The DFT total energies provide the internal energy (ground state) of the system.

In the present study, the main goal is to reflect on the chemical trends. Therefore, Eq. (2) can be written as:

$$\gamma(\mathrm{T}, p) = \frac{1}{2\mathrm{A}}[E^{\text{Total}}(\text{slab}) - n_{Ti}\mu_{\mathrm{Ti}}(\mathrm{T}, p) - n_X\mu_{\mathrm{X}}(\mathrm{T}, p)] \tag{3}$$

The results of Eq. (3) depend on the choice of chemical potentials for Ti and X. The chemical potential can be accurately estimated provided by the fact that the exact conditions of the system and its surrounding is known for the actual chemical reaction which involves the knowledge of the mechanism and intermediate steps. Therefore, assigning a precise value of the chemical potentials can be challenging. This has also been highlighted in a recent publication where various substitutional defects in Ti were analyzed using similar techniques [43]. That being said, the allowed range of chemical potentials can be defined quite accurately through the consideration of enthalpy of formation of the compounds and/or through mapping of chemical potential data available in thermochemical data tables. Since Ti is in the solid state under atmospheric conditions below its melting point, the chemical potential of Ti can be considered as a constant and independent of pressure.

Maximum and minimum chemical potentials for O, N, H can be derived from O_2, N_2 and H_2 molecules, which can be expressed through the following relations:

$$\mathrm{Max}[\mu_{\mathrm{X}}(\mathrm{T}, p)] = \frac{1}{2}E^{\text{Total}}_{\mathrm{X_2}} \tag{4}$$

$$\mathrm{Min}[\mu_{\mathrm{O}}] = \frac{1}{2}\left[E_{\mathrm{TiO_2}}(\text{bulk}) - \mu_{\mathrm{Ti}}\right] \tag{5}$$

$$\mathrm{Min}[\mu_{\mathrm{N}}] = [E_{\mathrm{TiN}}\ (\text{bulk}) - \mu_{\mathrm{Ti}}] \tag{6}$$

$$\mathrm{Min}[\mu_{\mathrm{H}}] = \frac{1}{2}\left[E_{\mathrm{TiH_2}}(\text{bulk}) - \mu_{\mathrm{Ti}}\right] \tag{7}$$

$$\Delta\mu_{\mathrm{X}}(\mathrm{T}, p) = (\mathrm{Max}[\mu_{\mathrm{X}}(\mathrm{T}, p)] - \mathrm{Min}[\mu_{\mathrm{X}}(\mathrm{T}, p)]) \tag{8}$$

$\Delta\mu$ in Eq. (8) is bounded by enthalpy of formation of TiO_2, TiN and TiH_2 compounds as in Eq. (5-7), respectively, and Eq. (4). Min[μ_X] are obtained from Eq. (5-7), respectively, and are independent of temperature and pressure. A more elegant way to treat the chemical potentials is by using the thermochemical data of O_2 and N_2 gases, which have been documented extensively in thermochemical data books [44]. The chemical potential as a function of temperature and partial pressure is given by;

$$\mu(\mathrm{T}, p) = \mu(\mathrm{T}, p^0) + (1/2)k_B\mathrm{T}\ln(p/p^0), \tag{9}$$

where, p^0 is the reference pressure at 1 atmosphere and k_B is the Boltzmann's constant. It is more appropriate to use Eq. (8) for the chemical potential of gases since the surface energy can be expressed as a function of T and p. This approach has been employed in our DFT based thermodynamic analysis. In the present study, the temperature dependence of chemical potentials of O and N are derived from the enthalpy and entropy from thermodynamic data tables as [44]:

$$\mu_{\mathrm{X}} = 1/2[(H(T, p^0, \mathrm{X_2}) - H(0\ K,\ p^0, \mathrm{X_2})) - T(S(T, p^0, \mathrm{X_2}) - S(0\ K,\ p^0, \mathrm{X_2}))] \tag{10}$$

respectively. The chemical potentials for some of the common gases, H_2, N_2 and O_2, obtained from Ref. [44] are shown in Fig. 2 as a function of temperature, where the allowed range of chemical potential at a desired temperature, for example at 4000 K for O_2, is determined from the graph by matching a vertical arrow starting from the reference line at zero to (black horizontal line) the value of chemical potential at that particular temperature.

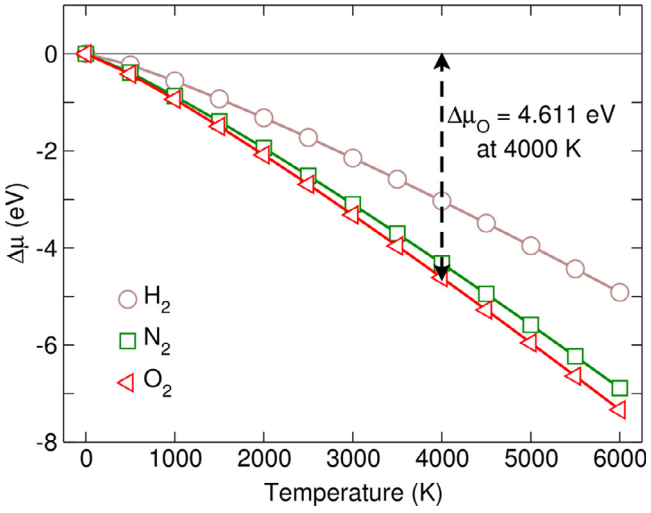

Fig. 2. The range of chemical potentials for H_2, N_2 and O_2 as computed using Eq. (8) and the data available in thermochemical data table. The double arrow vertical dashed line shows the allowed range of chemical potential for O_2 at 4000 K.

3. Results and discussion

3.1. Ground state properties of O and N adsorption on Ti

Oxygen, nitrogen and hydrogen atoms are adsorbed on a (0001) Ti surface with increasing concentrations of each element. The energetically most stable structure for each of concentration is determined by considering all possible distributions of X = O, N, or H atoms. The 10 Ti layers slab model is denoted as 10[*Ti*], where hydrogen passivation of one of the surfaces inherently exists. The exposed clean surface is exactly opposite to the hydrogen passivated surface which is illustrated in Fig. 1. Incorporation of atoms of element X is described by the choice of element X and the corresponding layer concentration y as X_y. The concentration y is the ratio of the number of X atoms in the layer to the number of Ti atoms in a layer. The advantage of using such a description is the usefulness of showing the precise position of X in the Ti layers. For example, if an O atom with a surface concentration of y is positioned two layers deep into the Ti from the top, the model is represented as 8[Ti]$O_{0.11}$2[Ti]. The indexing of the layers is done starting from the top layer opposite to the passivated surface as index 1. The use of subscript is reserved to denote the concentration. It is important to note at this point that X atoms are found to be highly stable in the interlayer interstitial regions over the substitutional site. For the case of pure (0001) Ti slab, the optimized structure leads to a change in the interlayer distances exhibiting both inwards and outwards relaxation along the z-direction depending on the layer index. The z relaxation is compared to the interlayer separation along the z-direction of the bulk lattice, $d_{\langle 0001\rangle} = 2.32$Å, in order to calculate the relative change $[(d_{\text{inter}-\text{layer}} - d_{\langle 0001\rangle})/d_{\langle 0001\rangle}]$. According to this expression, the inward inter-layer relaxation is negative, while the outward inter-layer relaxation is positive. The relative inter-layer separation expressed in percent is shown as black solid line in Fig. 3 (a-b). It is observed that the top most layer (L_1 in Fig. 1) undergoes an inward relaxation. It has the highest magnitude of relaxation as compared to other inner layers. The inter-layer separation between 2nd (L_2 in Fig. 1) and 3rd (L_3 in Fig. 1) layers show a positive value implying an outward shift between the blocks 8[Ti] and the top block 2[*Ti*].

The charges of the surface layer converge to zero towards the vacuum. This is shown by surface integration of the charge density and is defined as:

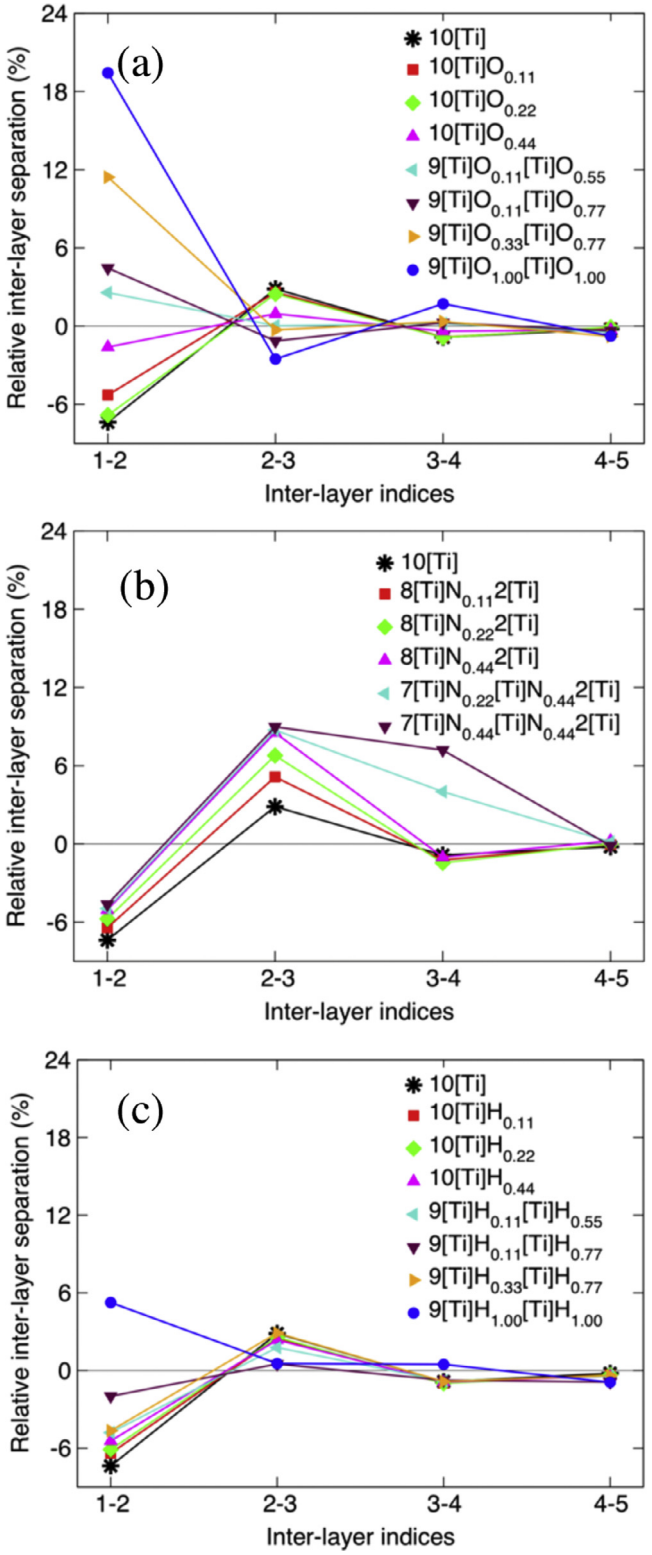

Fig. 3. Average inter-layer separation in relaxed slab models with increase in O, N and H concentrations in (a), (b) and (c), respectively. The low energy configuration for each of the concentrations is used for the structural analysis. For O and H adsorbed cases, the surface layer tends to move outwards with increase in O and H atoms, while for N adsorbed case, the N atoms penetrate two layers into the lattice. The structural configurations are suitably named to represent positions of O, N and H atoms in the slab models.

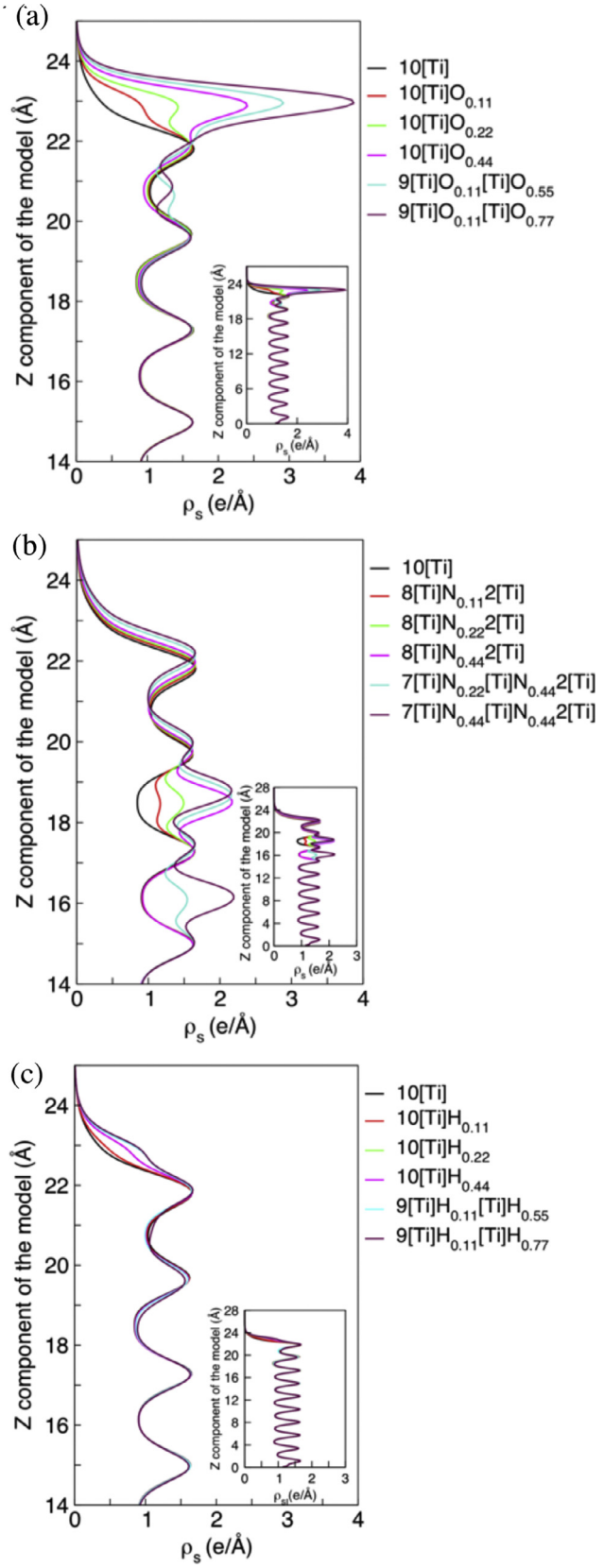

Fig. 4. Areal integration of charge density as a function of z-component of the slab model for O adsorbed Ti slab (a), N adsorbed Ti slab (b) and H adsorbed Ti slab (c). The inset shows the complete scale of the z-component. The charges are accumulated on the surface layer in the O and H adsorbed case which is associated with the adsorption of these atoms on the top Ti layer. Similarly, the charges are accumulated in the interior layer for N adsorbed case which is due to the occupancy of N atoms in the interior Ti layers.

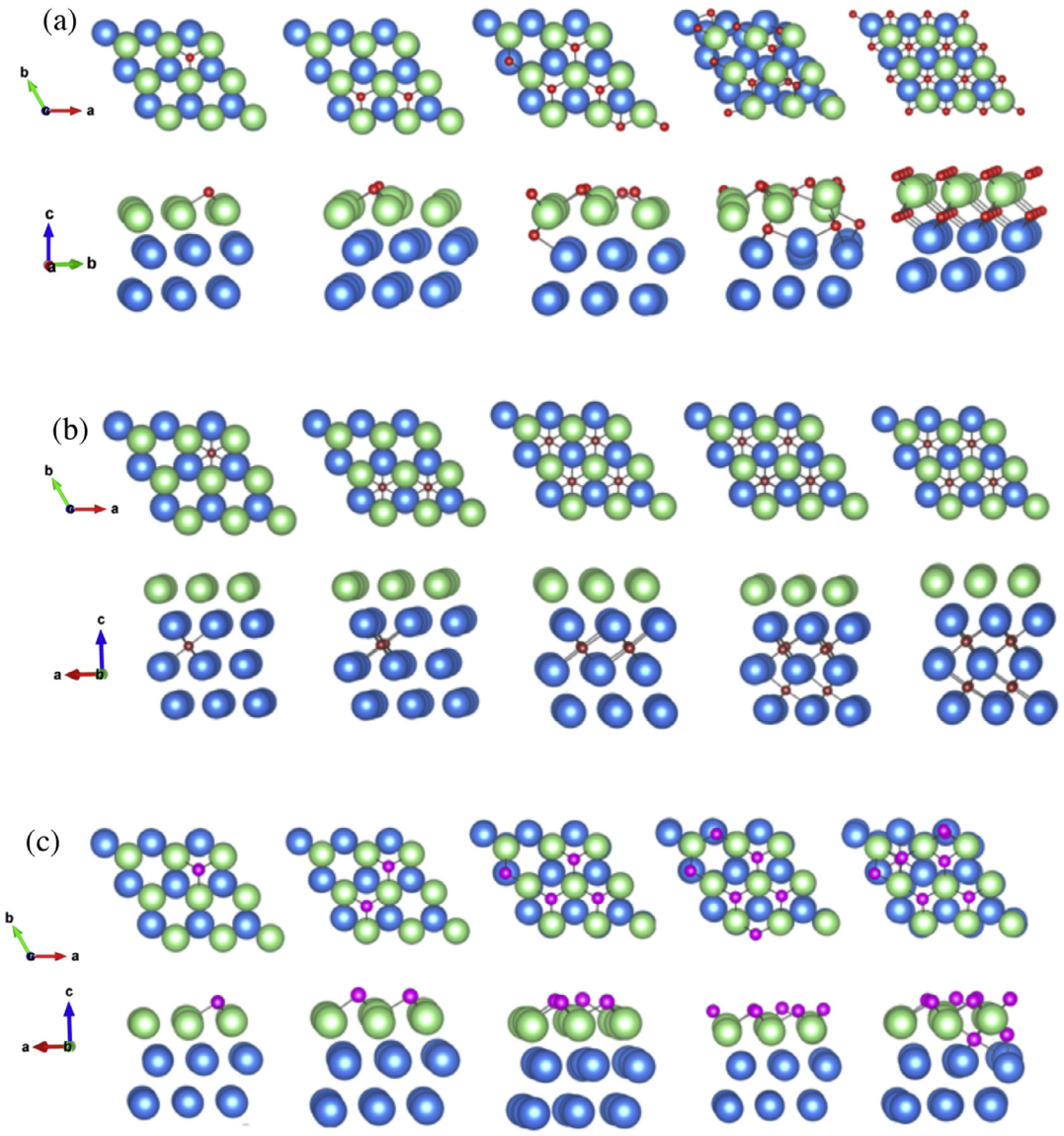

Fig. 5. Stable adsorbed geometries for Ti-O (a) and Ti-N (b) and Ti-H (c) systems for various concentrations. The top three Ti(0001) layers are shown, among which the blue and the light green balls represent atoms in the interior layers and the top Ti layer, respectively. Oxygen, nitrogen and hydrogen atoms are represented by red and maroon and magenta spheres, respectively.

$$\rho_S(z) = \iint \rho_V(z)dx\ dy \tag{11}$$

where ρ_V is the charge density obtained from the DFT calculations, as a function of z for the 10[Ti] as black line in Fig. 4(a-c).

The low energy configurations for each concentrations of O, N and H are shown in Fig. 5(a-c), respectively, which are determined from various atomic distributions of the corresponding elements. The ground state configurations for 1, 2, 4, 6 and 8 O, N and H atoms in the slab model are provided in Table 1. We found that both O and H atoms prefer to be adsorbed on the surface Ti layers until the surface is coated with one monolayer of O or H atoms. Further availability of O or H atoms will obviously lead to the migration of O or H towards the interior of the surface. For the case of N, however, there is a tendency for diffusion of N atoms in to the deep layers. As a function of concentration, the O, N and H adsorbed cases show varying tendencies of interlayer relaxations as illustrated in Fig. 3 (a-c). We found that for O and H case, the top three layers (denoted as L_1-L_3 in Fig. 1) undergo significant interlayer relaxations where the top two layers (the distance between L_1 and L_2) have significant inward relaxations, especially at low O and H concentrations. With further increasing concentrations of O the interlayer separations converge towards positive values indicating a strong outward relaxations. However, for H such outward relaxation is relatively weak. On the other hand, for N case, the inter-layer separation of the inner layer is most affected especially the layers where N occupancy is most preferable. In this case, the change of the inter-layer separation between layers 2 and 3 varies from almost zero to positive values as in Fig. 3(b). The two outer layers keep a similar qualitative trend like pure Ti surface. This is opposite to the layer relaxation with

Table 1
Terminologies for various ground state configurations of Ti-(O, N, H) systems containing 1, 2, 4,6 and 8 atoms.

No. of atoms	O	N	H
1	10[Ti]$O_{0.11}$	8[Ti]$N_{0.11}$2[Ti]	10[Ti]$H_{0.11}$
2	10[Ti]$O_{0.22}$	8[Ti]$N_{0.22}$2[Ti]	10[Ti]$H_{0.22}$
4	10[Ti]$O_{0.44}$	8[Ti]$N_{0.44}$2[Ti]	10[Ti]$H_{0.44}$
6	9[Ti]$O_{0.11}$[Ti] $O_{0.55}$	7[Ti]$N_{0.22}$[Ti] $N_{0.44}$2[Ti]	9[Ti]$H_{0.11}$[Ti]$H_{0.55}$
8	9Ti[Ti]$O_{0.11}$[Ti] $O_{0.77}$	7[Ti]$N_{0.44}$[Ti] $N_{0.44}$2[Ti]	9Ti[Ti]$H_{0.11}$[Ti] $H_{0.77}$

oxygen adsorption. With increasing nitrogen concentration, the surface relaxation shows opposite trend to that of pure Ti. For example, the top two layers relax outwards with magnitude proportional to the number of adsorbed O atoms, while the inner-layer separation between layers 2 and 3 switch from positive towards negative values. The inter-layer relaxations become negligible as one moves to inner layers for all adsorbed cases and converge approximately to that of the clean Ti surface.

A direct consequence of the ground state configuration and the inter-layer relaxation is on the distribution of the charge density. Position dependent charge distributions $\rho_S(z)$ defined in Eq. (11) for different concentrations of O, N and H for the slabs are shown in Figs. 4(a-c), respectively. It is revealed that oxygen has a strong tendency to accumulate charge density on the surface layers unlike that of N and H. This is due to the large electronegativity of O atoms (3.44 in Pauling units) compared to N (3.04), H (2.02) and its corresponding ground state geometry configuration where O atoms are preferred on the (0001) Ti surface. Due to the large electronegativity, the O atoms easily draw electrons from Ti which has a relatively smaller electronegativity (1.54). As a consequence, sharp peaks in the $\rho_S(z)$ appear within 22–24 Å for this case as shown in Fig. 4(a). On the other hand, for N case (Fig. 4(b)), the charge accumulation is noted in deeper layers of Ti surface. Although N has a similar electronegativity as O, its position in the octahedral interstitial positions of the inner layers provides a well-coordinated surrounding that results in maximizing hybridization. As a consequence, $\rho_S(z)$ does not exhibit any sharp variation as predicted for the case of O adsorption. For the case of H, however, no sharp peaks in $\rho_S(z)$ is observed as both H and Ti have nearly comparable values of electronegativities. This leads to similar $\rho_S(z)$ as obtained for Ti interior layers which is shown in Fig. 4(c).

3.2. Surface spin polarization

One of the interesting results obtained from our studies is the spin-polarization on surfaces. For the case of pure Ti surface, the total magnetic moment was found to be 3.50 μ_B. Fig. 6(a) shows the total magnetic moment for the reference Ti surface as well as for the low energy compositions for O and N atoms, where for the sake of clarity, the magnetic moment is reported per slab and the number of O and N atoms in the model is shown in the x-axis. Layer resolved magnetic moment analysis shows anti-parallel arrangement of magnetic moment, which is found for the top three layers, as, m_1: m_2: m_3 = 4.37 μ_B: − 0.86 μ_B: 0.08 μ_B [black lines in Figs. 6(b-d). From Fig. 6(a), it is evident that with increasing O concentration to 4 atoms, the spin polarization of Ti surface is compensated. This is not the case for N adsorption, where the magnetic moment was found to be slightly enhanced with increasing number of N atoms. For H case, the magnetic moment follows a similar qualitative trend like that of O case, where with increasing H concentration, the moment initially increases and with increasing concentrations, the system becomes magnetic by exhibiting non-vanishing moments (~3 μ_B). This is in contrast to the O-case. The explanation of the difference in trends for O and N adsorbed case can be provided by the difference in the ground state structures (associated with the trends in layer relaxations), with the fact that N atoms would be inclined to migrate towards the interior of the surface and that for the pure Ti the spin-polarization is carried mostly by the top two surfaces.

It is found that the magnitude of magnetic moment of the top two Ti layers, shown as L_1 and L_2 in Fig. 1, is reduced as the number of O or H atoms increases. On the other hand, with increasing N atoms, the top surface accumulates spin magnetic moment. However, in the second layer, no significant change in the magnetic moment is observed. These data with the ground state configuration show the role of O, H and H impurities in generating the desired structural reconstruction which may lead to a magnetic moment on Ti surfaces. The degree of spin polarization can hence be tuned based on the choice and concentration of the gas adsorption.

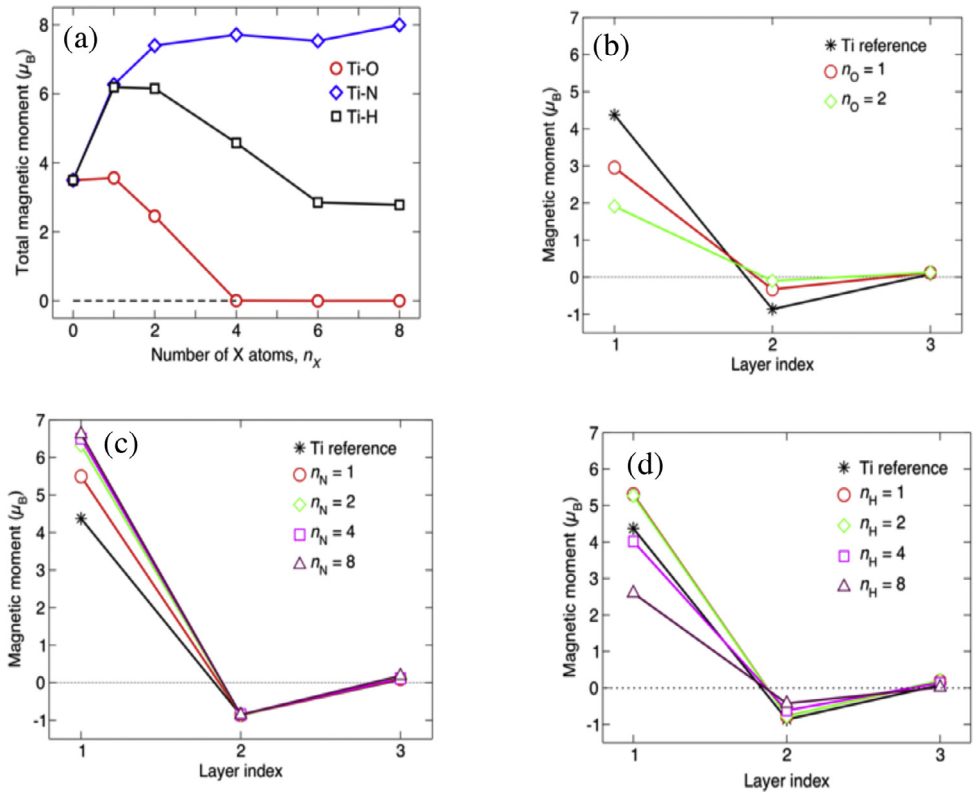

Fig. 6. (a) Total magnetic moment as a function of adsorbed O, N and H atoms for Ti-(O, N, H) systems. n_O, n_N and n_H, respecrtively. **(b), (c)** and **(d)** indicate the layer resolved magnetic moments for the top three layers for Ti-(O, N, H) systems, respectively. n_O, n_N and n_H denote the number of O, N and H atoms, respectively.

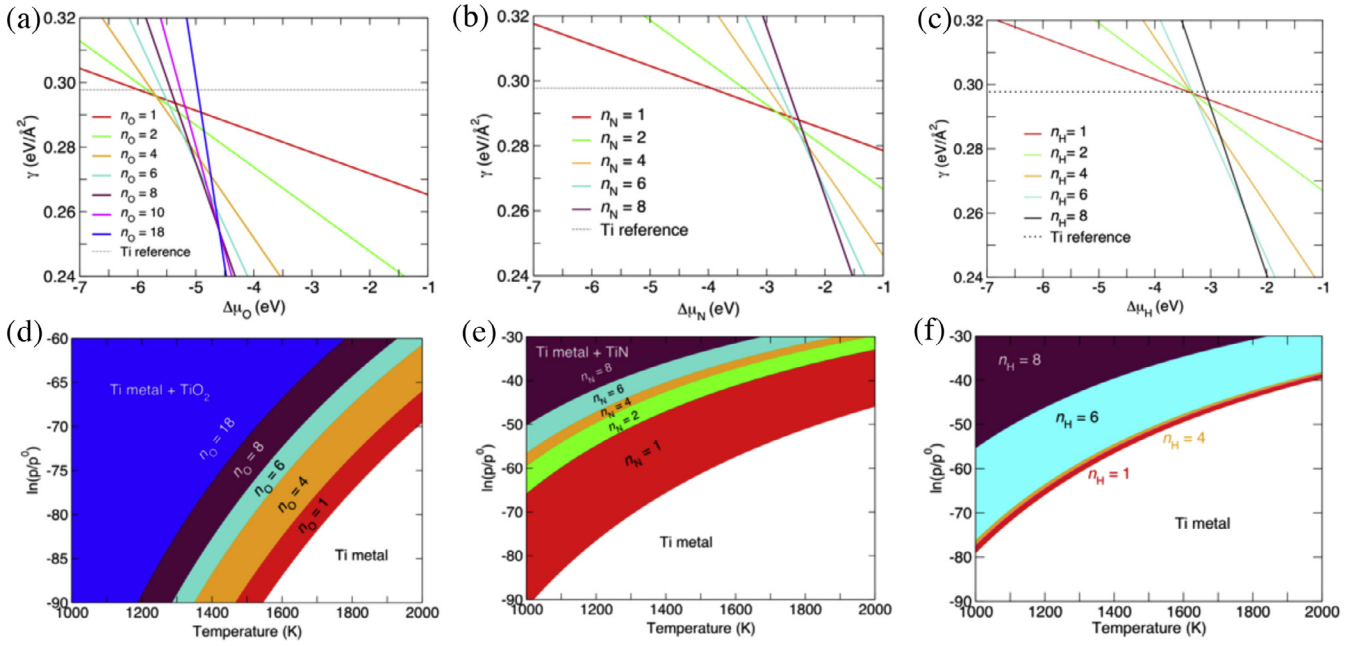

Fig. 7. Surface energy as a function of chemical potentials for different concentration of O adsorbed (a), N adsorbed (b) and H adsorbed (c) Ti slab. The graph of surface energy as a function of chemical potential is a straight line with the concentration, n_O and n_N, as its slope. The chemical potential at which two lines intersect represent the change in composition phase. The pressure and temperature dependence of composition obtained from the analysis of (a-c) are shown in (d-f) for O, N and H cases, respectively. Ti metal is found to be stable only at high temperature and low partial pressure of gases. In normal conditions, the surface is expected to be adsorbed by atoms of surrounding gases, this affinity is larger for oxygen as compared to nitrogen and hydrogen.

3.3. First-principles thermodynamics and phase stability diagrams

In order to investigate the influence of T and p on the stability of the adsorbed structures, we adopted an *ab-initio* thermodynamics approach [45]. The details of this procedure was provided in the computational method section. As a first step, using Eq. (3), γ as a function of $\Delta\mu_X$ as defined in Eq. (8) is computed for the adsorbed structures. Figs. 7 (a-c) illustrate the variation in γ as a function of oxygen, nitrogen and hydrogen chemical potentials obtained from the thermochemical data and using Eq. (10), respectively. This yields a straight line where the negative slope represents the concentration (number of O, N and H atoms, n_O, n_N and n_H, respectively). The low energy configurations for each concentration are always taken into consideration. The line with lower surface energy is considered more stable for that value of chemical potential. The crossing of the lines represents the chemical potential at which the system exhibits equal energy for two different concentrations of O or N or H. In other words, the concentration change is allowed at this particular chemical potential without the cost of any additional energy, and hence favours a change in the different compositions. Since the chemical potential is a function of pressure and temperature, the concentration change can be triggered with the right choice of partial pressure of the gas and the temperature of the system. Using Eq. (9), the surface energy is plotted as a function of $\ln(p/p^o)$ and temperature, where the line of intersection from Figs. 7(a-c) are represented as the crossover of different compositions in Fig. 7(d-f).

From Fig. 7(a-c), the crossover lines for O cases appear at approximately twice the chemical potential values than for the crossover of lines for N and H. The consequence of such change in the chemical potential values is reflected in the scale of pressure in the *y*-axis of Fig. 7(d-f), where the composition changes of Ti-O case can happen at very low partial pressure of O_2 gas in the range between (10^{-90} to 10^{-60}) atm as compared to the composition change of Ti for N or H induced by N_2 or H_2 gas partial pressure which is in the range between (10^{-90} to 10^{-30}) atm for N_2 and (10^{-80} to 10^{-30}) atm for H_2. Please note that the values of O_2, N_2 and H_2 partial pressures may not be directly correlated to the experimental values as the effect of entropy and vibrational energy are neglected in the calculations. The stable configurations obtained for large concentrations of O (9[Ti]$O_{0.11}$[Ti]$O_{0.55}$, onwards) and N (7[Ti]$N_{0.22}$[Ti]$N_{0.44}$2[Ti], onwards), see Fig. 5(a-b), hint towards the formation of TiO_2, while for Ti-N case, the migration of N towards the interior Ti layers gives the hint about the formation as well as the high stability of TiN. On the other hand, for Ti-H case, with concentrations, 9[Ti]$O_{0.11}$[Ti]$H_{0.55}$, onwards, we get a hint for the formation of TiH and TiH_2 phases with fluorite structure, [25,26] as shown in Fig. 5(a), which is highly stable in the bulk phase.

Our findings reveal that for Ti-O case, a clean Ti surface is only possible at relatively high temperatures at $T \sim 1550$ K compared to the case for Ti-N and Ti-H-cases which are ~1000 K (N case) and ~850 K (H case). This indicates the big challenge in stabilizing the clean Ti surface for O relative to other gaseous atoms. Sharp changes in O, N and H stoichiometries are observed at T < 1550 K (O case), 1000 K (N case), 850 K (H case), respectively. For example, for Ti-O case, for $T \lesssim 1200$K, with O_2 partial pressure varying from 10^{-90} atm to 10^{-60} atm, the TiO_2 is found to be highly stable which has a resemblance with the native stable Rutile structure of Ti oxide. Our results agree with the fact that at ambient partial pressure of O_2 gas in the environment, the surface of Ti should always be covered by an oxide layer thereby passivating the Ti surface as has been observed experimentally [5,18]. On the other hand, for N-case, the pure Ti metal becomes highly stable at T ~1000 K onwards at P_{N2} varying between 10^{-90} atm to 10^{-50} atm. For H-case, the T is even lower (~850 K) to stabilize the clean Ti surface. Below 1000 K, and low N_2 partial pressure (in the range 10^{-90} atm to 10^{-50} atm), the changes in different nitrogen stoichiometries are found. Among various stoichiometries, for P_{N2} (10^{-90} to 10^{-70}) atm the Ti_2N has a wide stability range, whereas the others changes sharply. However, the nitride phase similar to the bulk TiN with the NaCl cubic structure is found to be stable only at relatively high PN_2 (10^{-50} to 10^{-30}) atm compared to O_2 and below 1000 K. Experimentally, at ambient T and partial pressure, two nitride compounds, namely, the TiN and Ti_2N are found to be highly probable [46]. Our findings also converge to a similar conclusion showing a good agreement with the experiments. On the other hand, for Ti-H case, we identify the

formation of TiH_2 and TiH phases but at extremely high H_2 partial pressures ($>10^{-50}$, onwards) which is in contrast to O_2 and N_2 cases.

We note that at such high temperature range, ab initio results may not be reliable, because the entropy contributions would be large, including phenomena such as kinetics and diffusion thereby contributing to the actual physics of surfaces. Nevertheless, these results provide trends that are intuitive and the role of chemical hybridization on the thermodynamics is apparent from such an analysis. In other words, the results suggest that it could be extremely difficult to stabilize clean Ti (0001) surface, which is expected to be contaminated by adsorption of the gaseous atoms in the environment. From our results it is clear that oxygen has more affinity to Ti(0001) surface than nitrogen and hydrogen. This agrees well with the measurements regarding the formation of stable oxide layer on Ti thereby leading to a surface passivation at ambient T and oxygen partial pressure. It also supports to the formation of stable oxide layer on Ti. We predict that the compositional changes can be achieved by changing the partial pressure of the surrounding gas and the temperature of the metal surface.

4. Conclusions

A combined first principles ground state and *ab initio* thermodynamics study is presented to develop further insight into the interactions of oxygen, nitrogen and hydrogen with Ti surfaces. The stable geometries of the models show that oxygen and hydrogen prefer adsorption on the top Ti surface and tend to migrate to the second layer only after the surface is saturated by one mono-layer of oxygen or hydrogen. This is different than the behavior of nitrogen, where the nitrogen atom is found to be more stable in the interior of Ti. Pure Ti slab was found to be spin-polarized due to the geometrical reconstruction of surface layers where the top layers move relatively inwards and the next layer moves relatively outwards. On adsorption of oxygen, the spin polarization can be quenched which is not the case for nitrogen adsorption. The trends in spin polarization is indirectly correlated to the O, N and H concentrations through the surface layer relaxations.

The temperature and pressure dependence of chemical potentials of oxygen, nitrogen and hydrogen gas is used to derive surface phase diagrams of Ti-O, Ti-N and Ti-H systems. It is found out that oxygen has a stronger affinity to Ti than nitrogen and hydrogen. In normal conditions, room temperature and 1 atm pressure, the adsorbed Ti surface is more stable than clean surface. Hence, stabilizing pristine Ti surfaces could be a significant challenge. The current study provides an atomistic/microscopic understanding on the surface adsorption processes in Ti which could assist in designing Ti surfaces specifically tailored for powder related processes in metallurgy and for catalysis.

Acknowledgements

The high performance computing (HPC) facility at University of Connecticut is acknowledged for providing the computational resources.

References

[1] K. Golibrzuch, N. Bartels, D.J. Auerbach, A.M. Wodtke, Annu. Rev. Phys. Chem. 66 (2015) 399.
[2] R.J. Madix, J. Vac. Sci. Technol. 13 (1976) 253.
[3] N.D. Lang, W. Kohn, Phys. Rev. B. 3 (1971) 1215.
[4] C. Paul, K. Liu X, Mater. Sci. Eng. R. 47 (2004) 49.
[5] C. Leyens, M. Peters, Titanium an Titanium Alloys, (2003).
[6] H.G. Spilker, G. Jänsch-Kaiser, N. Pérez, H.G. Spilker, G. Jänsch-Kaiser, N. Pérez, Titanium and titanium alloys, Corrosion Handbook, Wiley-VCH Verlag GmbH & Co. KGaA, Weinheim, Germany, 2012.
[7] D.W. Shoesmith, J.J. Noël, Corrosion of Titanium and Its Alloys, in: Shreir's Corrosion, 2010: pp. 2042–2052.
[8] C.-C. Ting, S.-Y. Chen, D.-M. Liu, Thin Solid Films 402 (2002) 290.
[9] O.U.O. Mota, R.A. Araujo, H. Wang, Physics Procedia 66 (2015) 576.
[10] S.-Y. Liu, F.-H. Wang, Y.-S. Zhou, J.-X. Shang, J. Phys.: Condens. Matter. 19 (2007) 226004.
[11] M.V. Kuznetsov, E. Shalaeva, Phys. Metal. Metallogr. 97 (2004) 485.
[12] P. Rochana, K. Lee, J. Wilcox, J. Phys. Chem. C. 118 (2014) 4238.
[13] L. Li, F.-L. Meng, X.-Y. Hu, L. Qiao, C.Q. Sun, H.-W. Tian, W.-T. Zheng, RSC Adv. 6 (2016) 14651.
[14] I. Vaquila, M.C.G. Passeggi Jr, J. Ferron, Appl. Surf. Sci. 93 (1996) 247.
[15] X. Liu, Fan Ji, RSC Advances 6 (2016) 71311.
[16] G. Lu, S.L. Bernasek, J. Schwartz, Surf. Sci. 458 (2000) 80.
[17] H. Flower, P. Swann, Acta Metall. 22 (1974) 1339.
[18] L.I. Vergara, M.C.G. Passeggi, J. Ferrón, Appl. Surf. Sci. 187 (2002) 199.
[19] I. Vaquila, M.C. Passeggi, J.J. Ferron, Phys. Rev. B. 55 (1997) 13925.
[20] Y. Takakuwa, S. Ishidzuka, A. Yoshigoe, Y. Teraoka, Y. Mizuno, H. Tonda, T. Homma, NIM B. 200 (2003) 376.
[21] I. Jauberteau, R. Mayet, J. Cornette, D. Mangin, A. Bessaudou, P. Carles, J. Jauberteau, A. Passelergue, Coatings 7 (2017) 23.
[22] B.A. Shafaay, S. Mahmoud, A.M. Al Saeedi, E.E.E.H. Hassan, IIJIT 2 (2014) 30.
[23] U.Kuhnhold Knoll, C.H. Moore, J. Mining, Y.K. Trans, M.E. Syrkin, Dyatkina, Treatise on Inorganic Chemistry, (1957), p. 44.
[24] B. Ohler, S. Prada, G. Pacchioni, W. Langel, J. Phys. Chem. C. 117 (2013) 358.
[25] H. Smithson, C.A. Marianetti, D. Morgan, A. Van der Ven, A. Predith, G. Ceder, Phys. Rev. B. 66 (2002) 144107.
[26] W.M. Mueller, J.P. Blackledge, G.G. Libowitz, U.S. Atomic Energy Commission., Metal hydrides (1968).
[27] W.E. King, A.T. Anderson, R.M. Ferencz, N.E. Hodge, C. Kamath, S.A. Khairallah, A.M. Rubenchik, Appl. Phys. Rev. 2 (2015) 41304.
[28] S.A. Khairallah, A.T. Anderson, A. Rubenchik, W.E. King, Acta Mater. 108 (2016) 36.
[29] L. Bian, Laser-Based Additive Manufacturing of Metal Parts, Taylor and Francis, 2017.
[30] J. Felipe Montoya, I. Ivanova, R. Dillert, D.W. Bahnemann, P. Salvador, J. Phys. Chem. Lett. 4 (2013) 1415.
[31] S. Bagheri, N. Muhd Julkapli, S. Bee Abd Hamid, The Scientific World Journal 2014 (2014), p. 1.
[32] S. Rtimi, O. Baghriche, R. Sanjines, C. Pulgarin, M. Ben-Simon, J.-C. Lavanchy, A. Houas, J. Kiwi, Appl. Catal. B, Environmental. 123 (2012) 306.
[33] Y. Kobayashi, Y. Tang, T. Kageyama, H. Yamashita, N. Masuda, S. Hosokawa, H. Kageyama, J. Am. Chem. Soc. 139 (2017) 18240.
[34] K. Reuter, C. Stampf, M. Scheffler, AB Initio Atomistic Thermodynamics and Statistical Mechanics of Surface Properties and Functions, Handbook of Materials Modeling, Springer, Netherlands, Dordrecht, 2005, p. 149.
[35] H.D. Shih, F. Jona, D.W. Jepsen, P.M. Marcus, The structure of the clean Ti(0001) surface, J. Phys. C: Sol. St. Phys. 9 (1976) 1405.
[36] J. Perdew, K. Burke, M. Ernzerhof, Phys. Rev. Lett. 77 (1996) 3865.
[37] J.P. Perdew, Phys. Rev. B. 33 (1986) 8822.
[38] A.D. Becke, Phys. Rev. A. 38 (1988) 3098.
[39] G. Kresse, J. Furthmüller, Phys. Rev. B. 54 (1996) 11169.
[40] G. Kresse, J. Furthmüller, Comput. Mater. Sci. 6 (1996) 15.
[41] G. Kresse, Phys. Rev. B. 59 (1999) 1758.
[42] E.S. Fisher, C.J. Renken, Phys. Rev. 135 (1964) A482.
[43] S.K. Nayak, C.J. Hung, V. Sharma, S.P. Alpay, A.M. Dongare, W.J. Brindley, R.J. Hebert, Npj Comput. Mater. 4 (2018) 11.
[44] M.W. Chase, NIST-JANAF Thermochemical Tables, 4th Edition, NIST-JANAF Thermochemical Tables 2 Volume-Set, Journal of Physical and Chemical Reference Data Monographs (1998).
[45] Reuter Karsten, Scheffler Matthias, Phys. Rev. B. 65 (2001) 35406.
[46] I. Shigematsu, M. Nakamura, N. Saitou, K. Shimojima, J. Mater. Sci. Lett. 9 (2000) 967–970.